Science of the Total Environment 980 (2025) 179501

Contents lists available at ScienceDirect

Science of the Total Environment

journal homepage: www.elsevier.com/locate/scitotenv

High-resolution dynamically downscaled projections of future extreme temperatures, heatwaves and exposure in Southeast Asia

Jianjun Yu [a,*], Aurel F. Moise [a], Sandeep Sahany [a], Venkatraman Prasanna [a], Xin Rong Chua [a], Chen Chen [a], Muhammad E.E. Hassim [a], Gerald Lim [b], Fei Luo [a], Anupam Kumar [a], Puyang Liu [c], Pavan Harika Raavi [a]

[a] Centre for Climate Research Singapore, Meteorological Service Singapore, National Environment Agency, Singapore
[b] Weather Services Division, Meteorological Service Singapore, National Environment Agency, Singapore
[c] Department of the Built Environment, College of Design and Engineering, National University of Singapore, Singapore

HIGHLIGHTS

- Dynamical downscaling of six CMIP6 models over Southeast Asia at 8 km resolution
- Rising temperature hotspots in the Mekong Delta, Sumatra and Borneo
- More frequent and prolonged heatwaves in the Maritime Continent
- Stronger and longer heat events in cities along the Strait of Malacca and Java

GRAPHICAL ABSTRACT

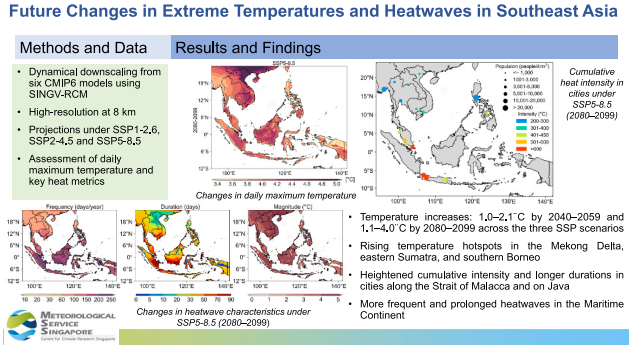

ARTICLE INFO

Editor: Anastasia Paschalidou

ABSTRACT

Extreme heat and heatwaves driven by global warming pose escalating risks globally, particularly in Southeast Asia (SEA), home to 680 million people, with a high concentration in urban areas. This study made use of CMIP6-based convection-permitting dynamically downscaled simulations at 8 km resolution over SEA under the three Shared Socioeconomic Pathways (SSP) scenarios: SSP1-2.6, SSP2-4.5, and SSP5-8.5. Projected changes in daily maximum temperatures and key heat metrics including the frequency of hotter days, heatwaves, and cumulative heat intensity and exposure time were analyzed across the region, as well as for individual countries and cities, for the near future (2040–2059) and far future (2080–2099) relative to the historical baseline (1995–2014). Results indicate a substantial rise in daily maximum temperatures over SEA, with average increases of 1.0–2.1 °C by 2040–2059 and 1.1–4.0 °C by 2080–2099 across the three scenarios. The Mekong Delta, eastern Sumatra and southern Borneo are identified as hotspots with pronounced temperature increase. More frequent and prolonged heatwaves are also projected over SEA, with heatwave frequency and duration doubling around 2025 and 2040, respectively, across the three scenarios, and increasing fivefold around 2045 and 2070, respectively, under SSP5-8.5. Specifically, the Maritime Continent is projected to face a notably higher frequency of hotter days,

* Corresponding author.
E-mail address: yu_jianjun@nea.gov.sg (J. Yu).

https://doi.org/10.1016/j.scitotenv.2025.179501
Received 19 January 2025; Received in revised form 2 April 2025; Accepted 20 April 2025
Available online 29 April 2025

establishing a new heat norm by the end of the century. Under SSP2-4.5 and SSP5-8.5, approximately 4 and 9 months/year, respectively, will be as hot as or hotter than the historical 5 % hottest days. Cities along the Strait of Malacca and on Java are expected to experience extreme heat with heightened cumulative intensity and longer durations. Mitigating emissions along a low-carbon pathway would provide substantial benefits for the Maritime Continent in the second half of the century, not only for human health but also for agriculture and ecosystems. This study provides the highest resolution and most updated projections of extreme heat over SEA to help inform targeted climate adaption strategies in this highly vulnerable region.

1. Introduction

Extreme heat events, characterized by temperatures significantly above normal, have widespread impacts on human health (Mora et al., 2017; Ebi et al., 2021), water resources (Hagemann et al., 2013), agriculture (Zhu et al., 2021; Lesk et al., 2022) and energy (Perera et al., 2020; Nik et al., 2021) sectors. These events also disrupt functioning of ecosystems (Ruthrof et al., 2018; Bastos et al., 2020) and critical infrastructure (Ke et al., 2016; Forzieri et al., 2018). Heatwaves, prolonged periods of such abnormally hot weather, amplify these diverse impacts. Catastrophic heatwaves have been documented worldwide, from Europe (Robine et al., 2008; Barriopedro et al., 2011; Yiou et al., 2020; Vautard et al., 2020) and Americas (Thompson et al., 2022) to Asia (Liu et al., 2021; Yoon et al., 2024; Aadhar and Mishra, 2023; Kim et al., 2024) and Australia (Coates et al., 2022). Notably, extreme heat associated with the 2023–2024 El Niño event shocked governments and individuals worldwide, with unprecedented temperatures recorded. Consequently, improved understanding, prediction and projection of extreme heat and heatwaves is important to inform policy preparedness.

Southeast Asia (SEA), home to 680 million people across eleven countries, with a high concentration in urban areas, is one of the fastest-developing and economically vibrant regions in the world. With agriculture serving as the backbone of economies and rapid industrialization and urbanization fueling its growth, this region is highly vulnerable to extreme heat and heatwaves due to high population density, widespread informal settlements and labor-intensive economy. Using ERA5 reanalysis dataset, Li (2020) analyzed the trend of heatwave characteristics over 1979–2018, and highlighted more frequent, longer-lasting, and stronger heatwaves would occur in SEA. Similarly, Muhammad et al. (2024) reported an increase in heatwaves over Peninsular Malaysia, particularly after 2000 and in the southeastern part of the region. Liu and Qin (2023) defined heatwaves using thermal indices and carried out an assessment from 1960 to 2020 over mainland SEA. This study found an increased trend, especially over the latest 30 years. In April and May 2023, SEA encountered a severe heatwave of 129-year return period, with record-breaking high temperatures exceeding 42 °C in many mainland SEA countries and a new record of 49 °C in Thailand (Lyu et al., 2024). This event built on SEA's history of severe heatwaves, making a new record after the major heatwave of 2016 (Thirumalai et al., 2017).

The world has witnessed an acceleration of extreme heat events, especially the occurrence of recent exceptional heatwaves. The temperature rise driven by global warming is undoubtedly to be worse in the future, highlighting the need for future climate change projections. Global climate models (GCMs), which simulate large-scale atmospheric and oceanic processes based on physical principles, have performed well in projecting future climate trends and extremes at continental and global scales. The sixth phase of the Coupled Model Intercomparison Project (CMIP6) has continued to improve these models by incorporating the latest knowledge of earth systems. The simulations for future emission scenarios have been instrumental in informing the Intergovernmental Panel on Climate Change Sixth Assessment Report (IPCC AR6) Working Group I. All GCMs consistently project a strong and accelerated increase in all extreme heat characteristics, including frequency, intensity and number of hot days etc., across nearly all inhabited regions (Domeisen et al., 2023). According to the IPCC AR6, the frequency of extreme temperature has risen from once every 10 years during 1850–1900 to approximately 2.8 (1.8–3.2) times at present, and projected to occur 5.6 (3.8–6.0) and 9.4 (8.3–9.6) times at 2 °C and 4 °C global warming levels, respectively (IPCC, 2021). The CMIP models have also been used to examine the projected changes in extreme temperatures and heatwaves with a focus on regional scales. In the context of SEA, Dong et al. (2021) analyzed CMIP5 projections and highlighted the increasing frequency and duration of heatwaves with higher extreme temperatures, noting distinct regional differences between the Maritime Continent and the Indochina Peninsula. Using CMIP6 models output, Sun et al. (2022, 2023) revealed a substantial rise in total population exposure to extreme heat and heatwaves over SEA, warning that contemporary younger generations will face heightened risks. Their research also showed regional inequality with largest increase in Indonesia and mitigation in the Philippines. Amnuaylojaroen et al. (2024) projected a significant increase in heat-related mortality across SEA under the high-emission scenario, by correlating to extreme temperature indices from ensemble mean of five selected CMIP6 GCMs.

While GCMs have been successful in informing climate change mitigation and adaptation strategies, regional climate models (RCMs), with spatial resolution of 50 km or finer, are still necessary for regional or localized studies. The use of dynamical downscaling techniques, which apply boundary conditions from coarse-resolution GCMs, allows for improved simulation of regional climate, particularly in regions with complex terrain, small islands, urban environment and diverse land surface types (Racherla et al., 2012). For examples, Zobel et al. (2017) explored dynamically downscaled regional projections of extreme temperatures and heat metrics across the continental United States. Similar high-resolution dynamical downscaling studies from CMIP6 GCMs have recently been conducted for Australia (Chapman et al., 2023) and New Zealand (Gibson et al., 2024). The Coordinated Regional Climate Downscaling Experiment for SEA (CORDEX-SEA) is a regional climate modeling initiative under the global CORDEX (Giorgi et al., 2009) framework. In its first phase, a total of 11 CMIP5 GCMs have been downscaled using 7 RCMs to a resolution of 25 km over the SEA domain (89.5°E–146.5°E, 14.8°S–27.0°N) for two different representative concentration pathways (RCP) scenarios, RCP4.5 and RCP8.5 (Tangang et al., 2020). Recent progress has been reported in identifying two independent groups of CMIP6 GCMs that align with expectations for dynamical downscaling over CORDEX-SEA (Nguyen et al., 2024).

The aim of this study is to investigate projected changes in future extreme temperatures, heatwaves, and heat exposure over SEA using a high-resolution regional climate model, SINGV-RCM, which dynamically downscales six CMIP6 GCMs at 8 km resolution (Prasanna et al., 2024). This study is the first up-to-date dynamical downscaling study over SEA based on the latest CMIP6 models. Compared to existing CORDEX-SEA experiments, our study uses a convection-permitting RCM for dynamical downscaling and provides additional climate change projections in SEA with a higher resolution and under multiple combined Shared Socioeconomic Pathways (SSP) scenarios. It can contribute to the research community by addressing the scarcity of high-resolution regional climate projections in this vulnerable region, providing a new dataset to deepen the understanding of complex tropical climate physics, uncertainties arising from RCMs and plausible SSP scenarios, to support climate change impact assessments and adaptation efforts. In this study, we will focus on assessing ensemble mean changes in

simulated daily maximum temperatures across the region and in individual countries. Additionally, we will analyze shift of temperature distributions to evaluate how heat extremes in the upper tail are affected by future warming. Based on these findings, we will examine how rising temperatures affecting key heat metrics, including heatwave characteristics, cumulative heat intensity and exposure time. The high-resolution regional climate projections provide added value by enabling a closer examination of heat metrics at the country and city level in SEA.

2. Materials and methods

2.1. SINGV-RCM: dynamical downscaling over SEA

A convection-permitting reginal climate model, SINGV-RCM, was developed as part of Singapore's Third National Climate Change Study (V3) for downscaling the sub-selected CMIP6 GCMs over SEA including Singapore. The SINGV-RCM is built on the dynamical core of the Met Office Unified Model (Met UM) version 11.1 with a science configuration specific to tropical climate physics (Bush et al., 2020). To conduct dynamical downscaling, SINGV-RCM was forced using the initial and lateral boundary conditions (6-hourly) along with 6-hourly Sea Surface Temperatures (SSTs) from the sub-selected GCMs over the SEA domain (16.16°S–24.08°N, 79.68°E–160.248°E) at 8 km resolution, with a time step of 4 min.

In order to carry out sub-selection we follow standard practices suggested by CORDEX (Gutowski Jr et al., 2016). Specifically, the sub-selected GCMs should: (1) span as much as possible the full range of GCM projections of temperature and precipitation over SEA across the CMIP6 ensemble, (2) perform satisfactorily in the historical climate as compared to observations and reanalysis for both key climate variables (e.g., temperature and precipitation) and key processes (e.g., monsoons, ENSO, IOD, MJO), (3) span the range of model diversity in terms of genealogy so that models from different families can be included, and (4) have 6-hourly lateral boundary conditions available to drive SINGV-RCM. Following the above methodology, we sub-selected 6 CMIP6 GCMs for downscaling, including ACCESS-CM2, EC-Earth3, NorESM2-MM, MIROC6, MPI-ESM1-2-HR and UKESM1-0-LL. Table 1 provides details of these sub-selected CMIP6 GCMs. For more details on the evaluation and sub-selection process, please refer to V3 Science Report, Chapter 5 (CCRS, 2024). For daily maximum temperature examined in this study, Fig. S1b presents climatological bias for the historical period (1995–2014) relative to SA-OBS (Van Den Besselaar et al., 2017), as shown in Fig. S1a. All selected GCMs exhibit a similar spatial pattern, with a warm bias exceeding +2 °C in high-altitude mountainous regions and a cool bias of more than −1 °C in plains, urban lowlands, swamps and rainforests. The root mean square error (RMSE) and mean absolute error (MAE) across the 6 GCMs range from 2.0 to 2.5 °C and 1.5 to 2 °C, respectively.

Dynamical downscaling was conducted using the above 6 GCMs for both historical (1955–2014) and future periods. The future projections cover the period from 2015 to 2100 for 3 combined SSP and mitigation targets (defined by radiative forcing levels with targeted atmospheric greenhouse gas concentrations) scenarios, as used in the IPCC AR6: SSP1-2.6, SSP2-4.5 and SSP5-8.5. The number of grid points for SINGV-RCM simulations over SEA is approximately 40 million (including horizontal and vertical), which takes around 16 min of wall clock time per simulated day using 768 CPUs. The total simulation time for the 8 km dynamical downscaling simulations is around 2 years, on two 10 Petaflop supercomputers, one at Singapore's National Supercomputing Centre (NSCC) and the other at the National Computational Infrastructure (NCI) in Australia. For more details, please refer to the V3 Science Report, Chapter 13 (CCRS, 2024).

Fig. 1 shows the spatial domain of SEA (between 94°E–142°E and 12°S–24°N) and 16 selected cities under investigation, which is a smaller area compared to full model domain. Geographically, this region encompasses the Indochina, Peninsula Malaysia, Sumatra, Borneo and Java, characterized by complex terrains, islands and coastlines. The V3 Science Report (CCRS, 2024) documented projected change in key climate variables such as rainfall, temperature, relative humidity, and wind speed.

2.2. Metrics

This study focuses on extreme temperatures, specifically daily maximum temperature (T_{max}), and related heat metrics, including heatwaves, cumulative heat intensity, and exposure time. Heat extremes are defined using a percentile-based approach, where the threshold is determined for each grid cell and for each RCM simulation by selecting the 95th percentile of simulated T_{max} during the historical baseline period (1995–2014). This threshold is then applied to analyze heat metrics across both historical and future periods to assess projected changes. To reduce potential biases from individual models, we primarily present ensemble mean changes in T_{max} and associated heat metrics across RCMs. The analysis examines two 20-year periods: the near future (2040–2059) and the far future (2080–2099), relative to the baseline, under three SSP scenarios: SSP1-2.6, SSP2-4.5 and SSP5-8.5. Model spread will be discussed in the context of uncertainties arising from different RCM simulations.

2.2.1. Probability density functions (PDFs)

The shift in PDFs for T_{max} from the historical period to the future serves as an indicator of the degree of future warming. Following Hansen et al. (2006) and Zobel et al. (2017), we built PDFs for normalized T_{max} for each of the six RCM simulations for the historical baseline and the two future periods, and for the three SSP scenarios. For each grid, the mean and standard deviation (SD) of T_{max} for the historical baseline was firstly calculated. Then, the daily T_{max} time series for the baseline and all future scenarios were normalized by subtracting the historical mean value and divided by the historical SD, as follows (Zobel et al., 2017):

$$\widetilde{T} = \frac{T_t - \overline{T}_h}{\sqrt{\frac{1}{n}\sum_{t=1,h}^{n}\left(T_{t,h} - \overline{T}_h\right)^2}}$$

where $\widetilde{T}$ represents the normalized T_{max} and T_t is the simulated T_{max} at time point t in either the baseline or future period. $T_{t,h}$ refers to the T_{max} during the baseline period from 1995 to 2014, with $n = 7305$ days in

Table 1
Details of selected CMIP6 GCMs for dynamical downscaling.

Model name	Institution	Resolution atmosphere (km)	ΔPrecipitation (%)	ΔMean surface air temperature (°C)	Reference
ACCESS-CM2	CSIRO, Australia	250	13.1	4.1	Bi et al. (2013)
EC-Earth3	EC-Earth-Consortium, Europe	100	17.1	3.6	Döscher et al. (2022)
MIROC6	MIROC, Japan	250	9.2	2.5	Tatebe et al. (2019)
MPI-ESM1-2-HR	MPI-M, Germany	100	12.9	2.6	Gutjahr et al. (2019)
NorESM2-MM	NCC, Norway	100	–1.6	2.9	Seland et al. (2020)
UKESM1-0-LL	Met Office Hadley Centre, UK	250	12.9	4.6	Senior et al. (2020)

Note. The projected change in precipitation and mean surface air temperature is the mean change averaged across grids covering Southeast Asian domain (16.16°S–24.08°N; 79.68°E–160.248°E) during period 2080–2099 under SSP5-8.5 scenario relative to baseline 1995–2014.

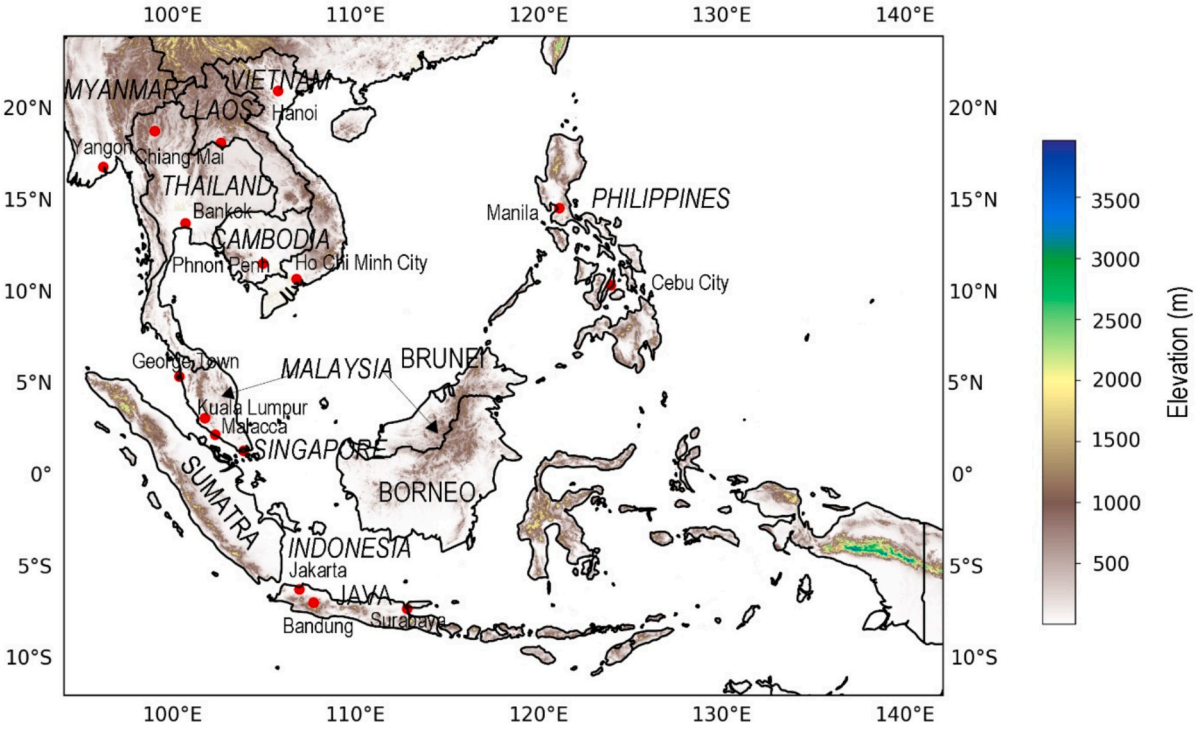

Fig. 1. Map of the study area in Southeast Asia.

total, which is used to calculate mean $\overline{T}_h$ and SD. The normalization aims to eliminate spatial differences in local climate for comparison. Theoretically, the constructed PDF for the baseline period should resemble a Gaussian-like curve with a zero mean value. Next, we plotted the baseline and future PDF curves that encompass all land grids over SEA for each RCM simulation, and determined the shift of the historical 95th percentile T_{max} (i.e., threshold to define heat extremes in the upper tail) by finding the corresponding percentile in the future PDFs where this value falls. The probability of exceeding the historical 95th percentile T_{max} can be approximated by subtracting the shifted percentile value from 100, which indicates the frequency of future days that will be as hot as or hotter than the historical top 5 % hottest days.

The interquartile range (IQR), defined as the difference between the 75th and 25th percentiles, is a widely used measure of distribution variability (Wilks, 2011). By examining the relative contributions of a shifted mean or IQR contributing to increased extreme heat events in the future, we can assess whether background warming or variability plays a more significant role in driving future extremes (Perkins, 2015). To quantify this, we constructed two new datasets based on the normalized historical daily maximum temperatures ($\widetilde{T}_{h,t}$) by adjusting either the mean (μ) or IQR while keeping other statistical characteristics unchanged, which can be expressed as follows:

$$\widetilde{T}_{mean-shifted,t} = \widetilde{T}_{h,t} + \left(\mu_f - \mu_h\right)$$

$$\widetilde{T}_{IQR-shifted,t} = \mu_h + \left(\widetilde{T}_{h,t} - \mu_h\right) \times IQR_f / IQR_h$$

where the subscripts h and f denote the historical and future periods, respectively. These two datasets were then used to build two interim distributions, representing PDFs that isolate the effects of mean shift and IQR change. Using the same threshold (i.e., the 95th percentile T_{max} in historical period), we computed the probabilities of exceeding this threshold for the four normalized daily maximum temperature distributions (i.e., historical, mean-shifted, IQR-shifted and future), denoted as P_h, P_m, P_{iqr} and P_f, respectively. Finally, we calculated the future risk ratio (RR_f) and decomposed it into contributions from mean shift (RR_m) and IQR change (RR_{iqr}) as follows:

$$RR_f = \frac{P_f}{P_h}$$

$$RR_m = \frac{P_m}{P_h}$$

$$RR_{iqr} = \frac{P_{iqr}}{P_h}$$

Comparing RR_m and RR_{iqr} provides insight into the dominant factor driving future heat extremes. These risk ratios were calculated for each RCM simulation, SSP scenario and time period, resulting in a total of 36 groups of values.

2.2.2. Heatwaves

A heatwave is defined as a sequence of unusual hot days, with thermal conditions exceeding a prescribed threshold based on local climatological conditions. In this study, a heatwave event is met when T_{max} exceeds a percentile-based threshold (i.e., 95th percentile of the RCM simulated T_{max} during historical baseline 1995–2014) for at least three consecutive days. Additionally, given the warm climate in SEA, the percentile-based threshold is set to a minimum of 30 °C to prevent overemphasis on projected heatwave increases in mountainous regions. The projected ensemble mean changes in heatwave frequency, duration, and magnitude are examined. Heatwave frequency is defined as the ratio of total heatwave days to the length of study period in days, equivalent to the empirical probability of heatwave occurrence. The duration of a heatwave in a given year is defined as the longest length in days of heatwave events. The heatwave magnitude is defined as the anomaly of the maximum temperature during heatwave days for a given year relative to the daily mean temperature over the baseline period.

To compare the heatwave frequency across different countries or regions, we adopt the annual event density (AED) metric to measure how often and how much a region is affected by heatwave events (Ridder et al., 2022). Firstly, for each calendar day, we calculated the percentage of the region affected by heatwaves, based on the fraction of

the number of grids experiencing heatwaves relative to the total number of grids within a country. These daily percentages were then summated for the entire year. In such a way, the value of AED was normalized to a range from 0 to 365 (or 366 for leap years), allowing for straightforward comparison of heatwave exposure among countries. A value of 0 indicates that nowhere experienced heatwaves in a given year, while a value of 365 (or 366 for a leap year) signifies everywhere in a country experienced heatwaves throughout the entire year.

2.2.3. Heat exposure

Prolonged exposure to extreme heat causes the human body's core temperature to rise. If physiological responses, such as increased skin blood flow and sweat rate, are insufficient to dissipate excess heat, the risk of heat-related morbidity and mortality (cardiovascular and respiratory) will be heightened. Without implementation of effective heat mitigation strategies, labor productivity of outdoor workers particularly in agriculture, construction and manufacturing sectors, is reduced, leading to economic loss. Additionally, financial burdens intensify due to the rising demand for cooling infrastructure and healthcare services. Beyond human health, excess heat impairs plant photosynthesis and affects animal thermoregulation, collectively threatening ecosystem stability.

We adopt cumulative heat intensity (CHI) and cumulative heat exposure time (CHT) as the metrics for assessing heat exposure (Perkins-Kirkpatrick and Lewis, 2020). CHI is defined as the cumulative heat exceedance over the extreme temperature threshold, expressed in degrees:

$$\mathrm{CHI} = \sum_{i=1}^{365} \max\left(0, T_{max,i} - T_{max95}\right)$$

where $T_{max,i}$ is the daily maximum temperature at ith day of the year, and T_{max95} is the 95th percentile of simulated daily maximum temperatures over historical baseline 1995–2014, as used for defining heatwaves in this study. A higher CHI value indicates a greater severity of heat exposure. CHT is total number of hours during which the hourly temperature exceeds the threshold, reflecting the duration of heat exposure:

$$\mathrm{CHT} = \sum_{i=1}^{365} \sum_{j=1}^{24} \begin{cases} 0 & \text{if } T_{i,j} < T_{max95} \\ 1 & \text{if } T_{i,j} \geq T_{max95} \end{cases}$$

where $T_{i,j}$ is the simulated temperature at the ith day and the jth hour.

The CHI and CHT were calculated for each modeling grid for all RCM

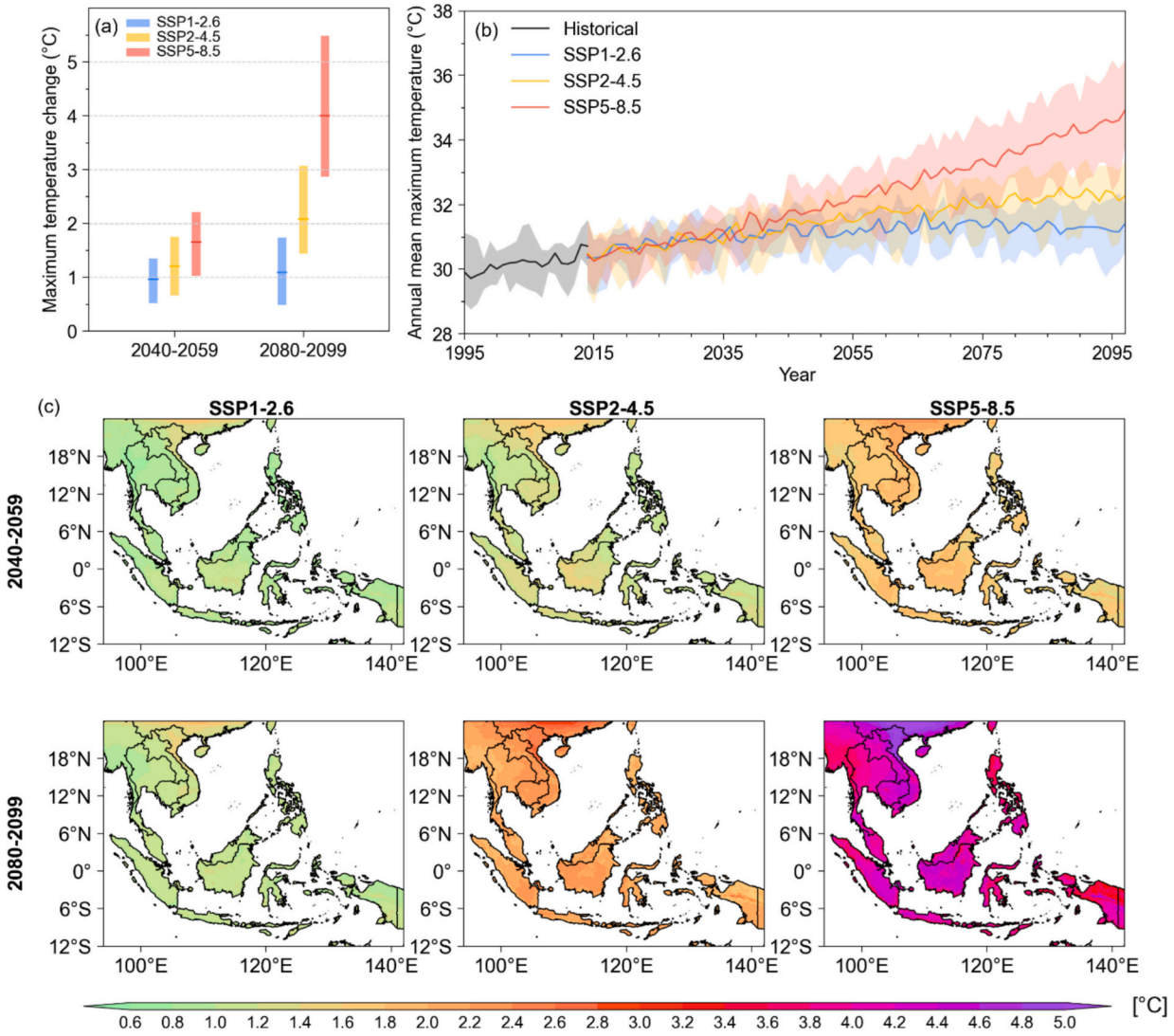

Fig. 2. Projected ensemble mean changes in daily maximum temperature over Southeast Asian land for 2040–2059 and 2080–2099 relative to the baseline from 1995 to 2014 (a); projected mean (solid line) and ranges (shading) for time series of annual mean daily maximun temperature from 1995 to 2099 (b); spatial distribution of projected change in daily maximum temperature in Southeast Asia (c).

simulations for both historical and future periods. We focused on assessing future heat exposure for 16 selected cities in SEA (Fig. 1), as these cities are vulnerable to extreme heat due to their high population density and social-economic importance. Firstly, we obtained spatial data in shapefile format from gadn.org and extracted the boundaries of the target cities. Next, for each RCM simulation, we overlaid these city boundaries with gridded historical and future CHI and CHT datasets to compute the average values for the grid cells encompassing each city. Finally, we calculated the ensemble mean CHI and CHT across all RCMs and determined the future-to-past change ratio to assess projected changes.

3. Results

3.1. Daily maximum temperature

The projected ensemble mean change in T_{max} averaged over SEA land is 1.0–1.1 °C under SSP1-2.6 for both the near and far future periods. As CO_2 emissions increase, T_{max} is expected to rise further to 1.2 °C under SSP2-4.5 and 2.1 °C under SSP5-8.5 during 2040–2059. By 2080–2099, this increase reaches to 1.7 °C and 4.0 °C, respectively (Fig. 2a). Fig. 2b shows the time series of annual mean T_{max} from 1995 to 2099, averaged across SEA land, along with the range of model spread. The projected annual mean T_{max} under all the three scenarios shows a similar increasing trend until 2040. Afterward, the T_{max} time series projected under SSP1-2.6 becomes stable and shows a slight decreasing trend by the end of the century. That for SSP2-4.5 stabilizes after 2080. The increasing trend of T_{max} under SSP5-8.5 is consistent until the end of the century, particularly showing a faster increase after 2050. The range of T_{max} time series increases slightly with time evolving, indicating higher uncertainty in future projections in the second half of the century. Geographically, the spatial pattern of T_{max} increase is consistent across different periods and scenarios, with a larger increase projected in northern Vietnam, the Mekong Delta, eastern Sumatra and southwestern Borneo (Fig. 2c). The variation in the projected T_{max} increase across the three SSP scenarios reflects the sensitivity of future T_{max} increases to rising CO_2 levels, with wider range indicating greater sensitivity to mitigation efforts. During 2040–2059, the variation in T_{max} increases ranges from 0.4 to 0.8 °C over the Maritime Continent and 0.8–1.1 °C over the Indochina Peninsula (Fig. S2a). It increases to over 2.4 °C across SEA by 2080–2099, with hotspots in northern Vietnam, Sumatra and Borneo (Fig. S2b). These results suggest that achieving carbon mitigation at lower levels can provide moderate benefits in limiting temperature increases over the Indochina Peninsula in the near-future and substantial benefits over northern Vietnam, Sumatra and Borneo towards the end of the century.

Table 2 shows the ensemble mean change in T_{max} for the listed nine SEA countries, which is averaged across the modeling grid cells encompassing each country, along with the range of model spread in bracket. During 2040–2059, the projected increase in T_{max} for the selected SEA countries is at a similar level across all three scenarios. Under SSP1-2.6, the T_{max} increases in these countries range from 0.8 to 1.1 °C, with an uncertainty spread of around 1 °C. The projected rise in T_{max} is 1.1–1.4 °C under SSP2-4.5, and 1.5–1.9 °C under SSP5-8.5. Differences in projected increases in T_{max} among countries are more prominent in the far future, particularly under SSP5-8.5. For example, countries on the Indochina Peninsula, such as Cambodia, Laos and Vietnam, show relatively higher T_{max} increases above 4.2 °C, comparing to equatorial countries like Brunei, Indonesia, Malaysia and Singapore, where T_{max} increases are projected to a range from 3.7 °C to 4.1 °C. The uncertainty remains at a similar level across all countries, with model spread ranging from 2.4 to 2.9 °C.

3.2. Shift in daily maximum temperature PDFs

Fig. 3 presents PDF curves of normalized T_{max} for SEA encompassing all land grids for the six SINGV-RCM simulations for the baseline and two future periods under the three SSP scenarios. The grey line represents the threshold for defining heat extremes, determined as the 95th percentile of the T_{max} distribution during the baseline period for each RCM simulation. The numbers in the top-right of each panel indicate the percentiles of this threshold value fallen in future PDF curves.

Under SSP1-2.6, the "cooler" models (i.e., MPI-ESM1-2-HR, Nor-ESM2-MM and MIROC6 driven SINGV-RCMs) exhibit a rightward shift in the mean by approximately 0.22–0.34 SD in the near-future PDFs, with a comparable shift in the far-future PDFs (Fig. 3c, d, and f). In both future periods, the historical 95th percentile value falls in a range from 87th to 91st, indicating that 9–13 % of days are projected to be as hot as or hotter than the historical top 5 % hottest days. The RR_{iqr} values for these RCM simulations remain within a range of 1–1.1, suggesting a negligible contribution of variability to the increase in future heat extremes compared to shifted mean, with RR_m values ranging from 1.6 to 2.2 (as listed in Table S1). In the contrast, the "warmer" models (i.e., UKESM1-0-LL, ACCESS-CM2 and EC-Earth3 driven SINGV-RCMs) show a larger rightward shift in the mean, ranging from 0.41 to 0.55 SD in the near future (Fig. 3a, b, and e). Combined with increased variability with IQR increases of 4–9 %, these models project 14–18 % hotter days during 2040–2059. By the end of the century, the mean shift in UKESM1-0-LL

Table 2
Projected changes in mean and the 95th percentile of daily maximum temperature for Southeast Asian countries.

Country	Period	ΔMean daily maximum temperature (°C)			Δ95th percentile daily maximum temperature (°C)		
		SSP1-2.6	SSP2-4.5	SSP5-8.5	SSP1-2.6	SSP2-4.5	SSP5-8.5
Brunei	2040–2059	0.9(0.5–1.5)	1.2(0.8–1.8)	1.7(1.1–2.5)	1.1(0.6–1.8)	1.4(0.8–2.0)	1.9(1.1–2.9)
	2080–2099	1.1(0.6–1.8)	2.1(1.3–3.2)	4.1(3.0–5.6)	1.2(0.4–2.2)	2.3(1.4–3.6)	4.5(3.1–6.4)
Cambodia	2040–2059	1.0(0.6–1.4)	1.2(0.7–1.9)	1.8(1.2–2.2)	1.1(0.6–1.5)	1.5(1.0–2.2)	1.8(1.4–2.2)
	2080–2099	1.1(0.5–1.9)	2.2(1.5–3.2)	4.3(3.3–5.7)	1.3(0.6–2.0)	2.4(1.5–3.5)	4.3(3.2–5.9)
Indonesia	2040–2059	1.0(0.6–1.4)	1.2(0.8–1.7)	1.6(1.1–2.2)	1.0(0.6–1.5)	1.3(0.8–1.8)	1.8(1.2–2.4)
	2080–2099	1.1(0.6–1.6)	2.0(1.3–2.9)	3.9(2.9–5.3)	1.1(0.6–1.7)	2.1(1.3–3.1)	4.2(3.0–5.7)
Laos	2040–2059	0.9(0.2–1.3)	1.2(0.5–2.0)	1.8(1.0–2.3)	1.3(0.6–1.9)	1.7(1.0–2.7)	2.0(1.6–2.5)
	2080–2099	1.1(0.3–1.9)	2.2(1.4–3.2)	4.2(3.0–5.9)	1.4(0.6–2.3)	2.7(1.6–4.0)	4.7(3.3–6.7)
Malaysia	2040–2059	0.9(0.6–1.4)	1.2(0.7–1.8)	1.6(1.1–2.4)	1.1(0.5–1.6)	1.4(0.7–2.0)	1.8(1.1–2.7)
	2080–2099	1.1(0.6–1.7)	2.0(1.3–3.1)	4.0(2.8–5.6)	1.2(0.5–1.9)	2.3(1.3–3.4)	4.5(3.0–6.3)
Philippines	2040–2059	0.8(0.4–1.2)	1.1(0.6–1.6)	1.5(1.0–2.1)	1.0(0.5–1.5)	1.3(0.8–1.8)	1.7(1.0–2.4)
	2080–2099	1.0(0.5–1.6)	1.9(1.3–2.8)	3.7(2.9–4.8)	1.2(0.6–2.0)	2.1(1.4–3.2)	4.1(3.0–5.6)
Singapore	2040–2059	0.9(0.6–1.3)	1.1(0.7–1.7)	1.5(0.9–2.2)	0.8(0.4–1.3)	1.1(0.7–1.7)	1.5(0.9–2.3)
	2080–2099	1.0(0.5–1.6)	1.9(1.3–2.9)	3.7(2.7–5.2)	1.0(0.4–1.6)	1.9(1.2–2.9)	3.7(2.7–5.3)
Thailand	2040–2059	0.9(0.3–1.3)	1.1(0.6–1.9)	1.7(0.9–2.2)	1.1(0.6–1.5)	1.5(0.9–2.2)	1.9(1.5–2.2)
	2080–2099	1.0(0.3–1.8)	2.1(1.3–3.1)	4.0(2.9–5.5)	1.3(0.7–1.9)	2.4(1.5–3.5)	4.3(3.1–6.0)
Vietnam	2040–2059	1.1(0.5–1.5)	1.4(0.6–2.1)	1.9(1.2–2.4)	1.3(0.6–1.8)	1.7(0.8–2.6)	2.1(1.4–2.6)
	2080–2099	1.3(0.4–2.0)	2.3(1.6–3.4)	4.5(3.2–6.1)	1.5(0.5–2.3)	2.7(1.5–4.0)	4.8(3.6–6.8)

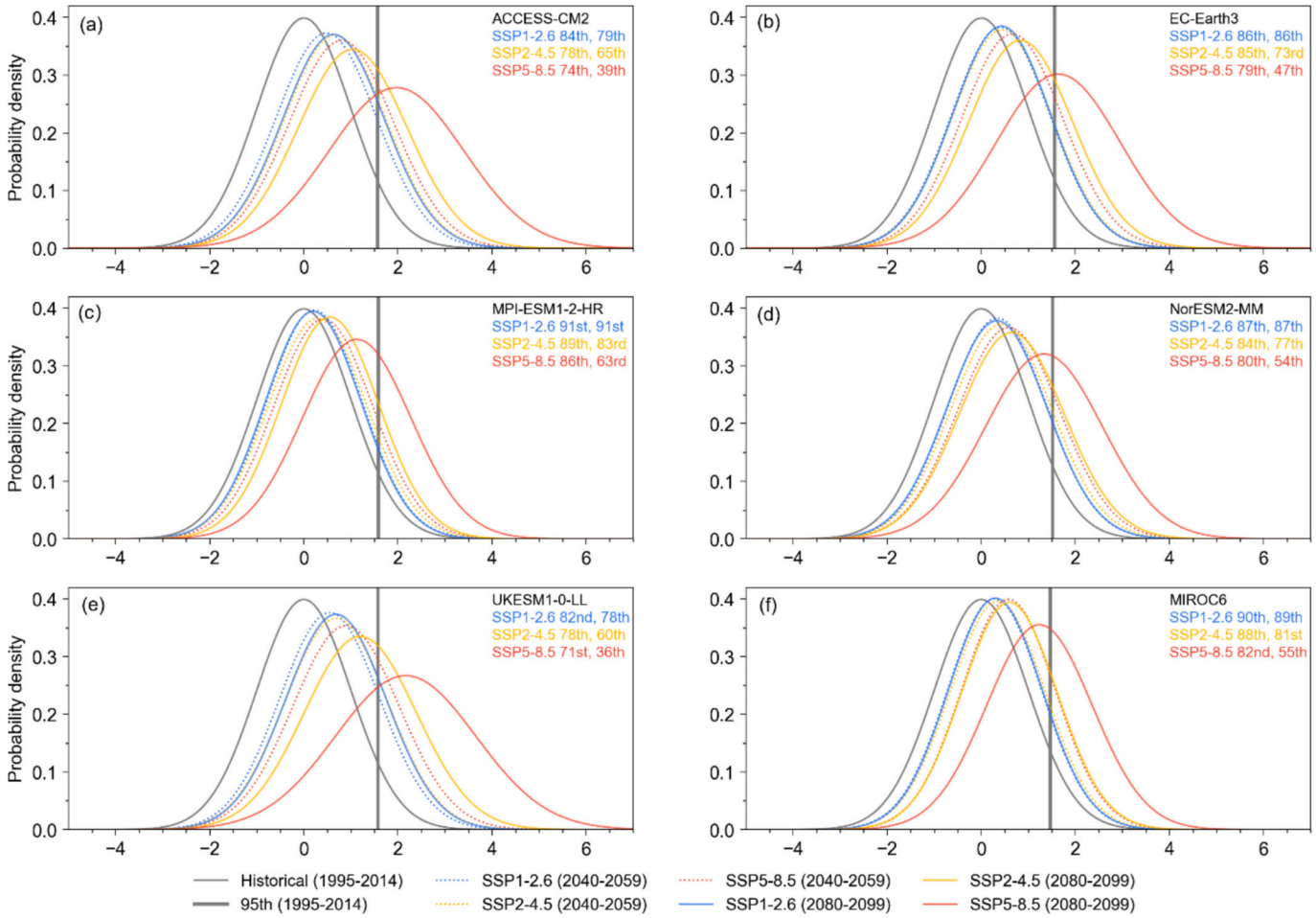

Fig. 3. Normalized daily maximum temperature distributions over Southeast Asian land for the baseline period (1995–2014) and near (2040–2059) and far future (2080–2099) periods from SINGV-RCM simulations driven by ACCESS-CM2 (a), EC-Earth3 (b), MPI-ESM1-2-HR (c), NorESM2-MM (d), UKESM1-0-LL (e), and MIROC6 (f). The grey line indicates the historical 95th percentile value. The numbers in the top-right indicate the percentiles of this value fallen in future distribution curves.

and ACCESS-CM2 driven simulations reaches 0.68 and 0.63 SD, respectively, leading to 21–22 % of days being hotter though variability remains stable with less than a 1 % increase in IQR compared to mid-century. Overall, background warming is the primary driver of future increases in hotter days under SSP1-2.6, with no change in variability (i.e., RR_{iqr} values remain close to 1), particularly for the "cooler" models.

The shift in both mean and variability of T_{max} increases with rising CO_2 under SSP2-4.5 and SSP5-8.5, intensifying from the near to far future. One major driver could be the expansion of the Indo-Pacific Warm Pool (IPWP). The growing IPWP sustains persistently high SSTs spanning from the western Pacific and eastern Indian Oceans, enhancing atmospheric moisture and heat transport into SEA land. Additionally, rising CO_2 concentrations strengthen the greenhouse effect, trapping more heat in the lower atmospheric, coupled with reduced cloud cover, resulting in rising surface temperature. Furthermore, in a warming climate, a stronger El Niño-Southern Oscillation (ENSO) prolongs extreme dry and heat events, while the shifts in Asian monsoon onset contribute to seasonal temperature variability. Collectively, these processes drives greater temperature variability across SEA. In the near-future PDFs, the mean shift in all RCM simulations ranges from 0.3 to 0.7 SD under SSP2-4.5, and from 0.4 to 0.9 SD under SSP5-8.5. The corresponding IQR increases by 5–13 % and 6–16 %, respectively, except for the coolest model (driven by MICROC6), which remains unchanged. These combined effects result in the historical 95th percentile value falling within the 78th to 89th percentile under SSP2-4.5 and the 71st to 86th percentile under SSP5-8.5, which translates to 11–22 % and 14–29 % hotter days, slightly greater than those projected under SSP1-2.6.

The difference in RCM projections grows in the far-future period, particularly under SSP5-8.5, primarily due to the strong response of "warmer" models (i.e., driven by UKESM1-0-LL and ACCESS-CM2) to CO_2 forcing and stronger cloud feedback, which originated from their parent GCMs. By 2080–2099, the value of RR_m is 3.5–3.8 times of RR_{iqr} for these models under SSP2-4.5, indicating that the shifted mean in T_{max} PDFs contributes approximately three to four times more to the future heat extremes than variability changes. This effect is amplified under SSP5-8.5, with RR_m values reaching 13.3 and 14.6, approximately 4.8 times higher than RR_{iqr}. This suggest that the warming trend is the dominant driver of future heat extremes, despite some degree of amplification from increased variability. As a result, these "warmer" models project a total of 35 % and 40 % hotter days under SSP2-4.5, respectively, compared to 19 to 27 % in the other models. The projected hotter days rises to 37 to 64 % under SSP5-8.5, highlighting a greater model uncertainty. Hence, when utilizing the projected heat extremes from this study for impact modeling or adaptation planning, particularly under a high-emission scenario and towards the end of the century, stakeholders should account for their risk tolerance without overlooking the model uncertainty in decision making.

Fig. 4a illustrates the spatial variation in the exceedance rate of the historical 95th percentile T_{max} across SEA, indicating the percentage of future days with T_{max} equivalent to or hotter than the top 5 % hottest days in the history. Most areas in the Indochina and Peninsula Malaysia

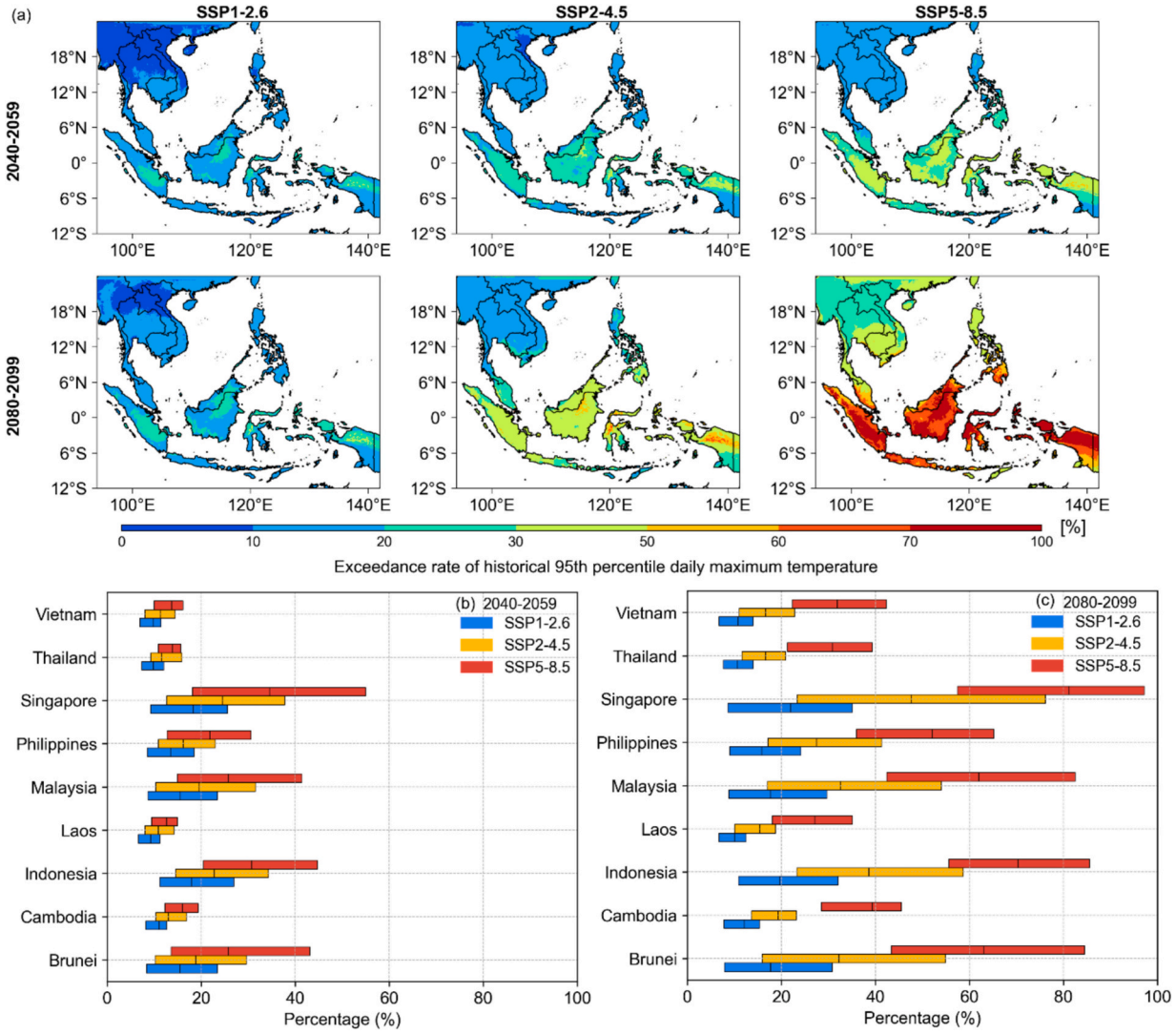

Fig. 4. Spatial distribution of projected exceedance rate of the historical 95th percentile daily maximum temperature averaged across RCMs (a) and ensemble mean and ranges of exceedance rate for the nine Southeast Asian countries for 2040–2059 (b) and 2080–2099 (c).

are projected to experience 10–20 % hotter days during 2040–2059 under all SSP scenarios. In southern Myanmar, northern Thailand, Laos and northern Vietnam, the models project less than 10 % hotter days under SSP1-2.6 scenario. In southern Peninsula Malaysia, over 20 % of future days are projected to be hotter under SSP5-8.5. By 2080–2099, the percentage of future hotter days in the Maritime Continent increases to 20–50 % under SSP2-4.5 scenario compared to 10–20 % in the Indochina Peninsula. Under SSP5-8.5, this could reach above 60 % in Malaysia's western coast, Sumatra, Borneo, and Java. Particularly, eastern Sumatra and southwestern Borneo are hotspots suffering a much higher frequency of extreme heat, seeing more than 70 % of days exceeding historical extreme heat level.

Fig. 4b and c illustrate the ensemble mean and range of the exceedance rate for the nine SEA countries during both near and far future periods. Generally, the Indochina countries (i.e., Cambodia, Laos, Thailand, and Vietnam) are expected to experience a lower frequency of hotter days in the future compared to the Maritime Continent countries (i.e., Brunei, Indonesia, Malaysia, Philippines, and Singapore). Additionally, uncertainty is lower in Indochina countries, showing a narrower range of model spread. For instance, the future hotter days for Indochina countries account for 9–16 % during 2040–2059, with a model spread of approximately 5–8 % across the three SSP scenarios. In contrast, the Maritime Continent countries are projected to have 14–35 % future hotter days, with an uncertainty range of 11–38 %. The detailed projections for each SEA country are listed in Table S2.

During 2080–2099, the Maritime Continent countries are anticipated to endure a significantly higher frequency of hotter days, reaching a level of 32–48 % and 62–81 % under SSP2-4.5 and SSP5-8.5, respectively. This establishes a new heat norm for this region by the end of the century, with T_{max} exceeding historical extreme levels (i.e., corresponding to 5 % occurrence frequency) for approximate 4 and 9 months per year, respectively. This is primarily because seasonal temperature variability is low in the Maritime Continent, characterized by a narrow and peaked distribution. As a result, the rightward shift of the temperature distributions could easily surpass the percentile-based threshold, increasing frequency of extreme heat events in the upper tail of the distribution. Despite this, the projected increase in extreme T_{max} at 95th percentile remains higher in the Indochina Peninsula. As indicated in Table 2, it increases by 2.4–2.7 °C and 4.3–4.8 °C in Cambodia, Laos, Thailand, and Vietnam under SSP2-4.5 and SSP5-8.5, respectively, by 2080–2099, which is approximately 0.5 °C higher than in Maritime Continent countries.

3.3. Heatwaves

Fig. 5a shows the spatial patterns of projected changes in heatwave

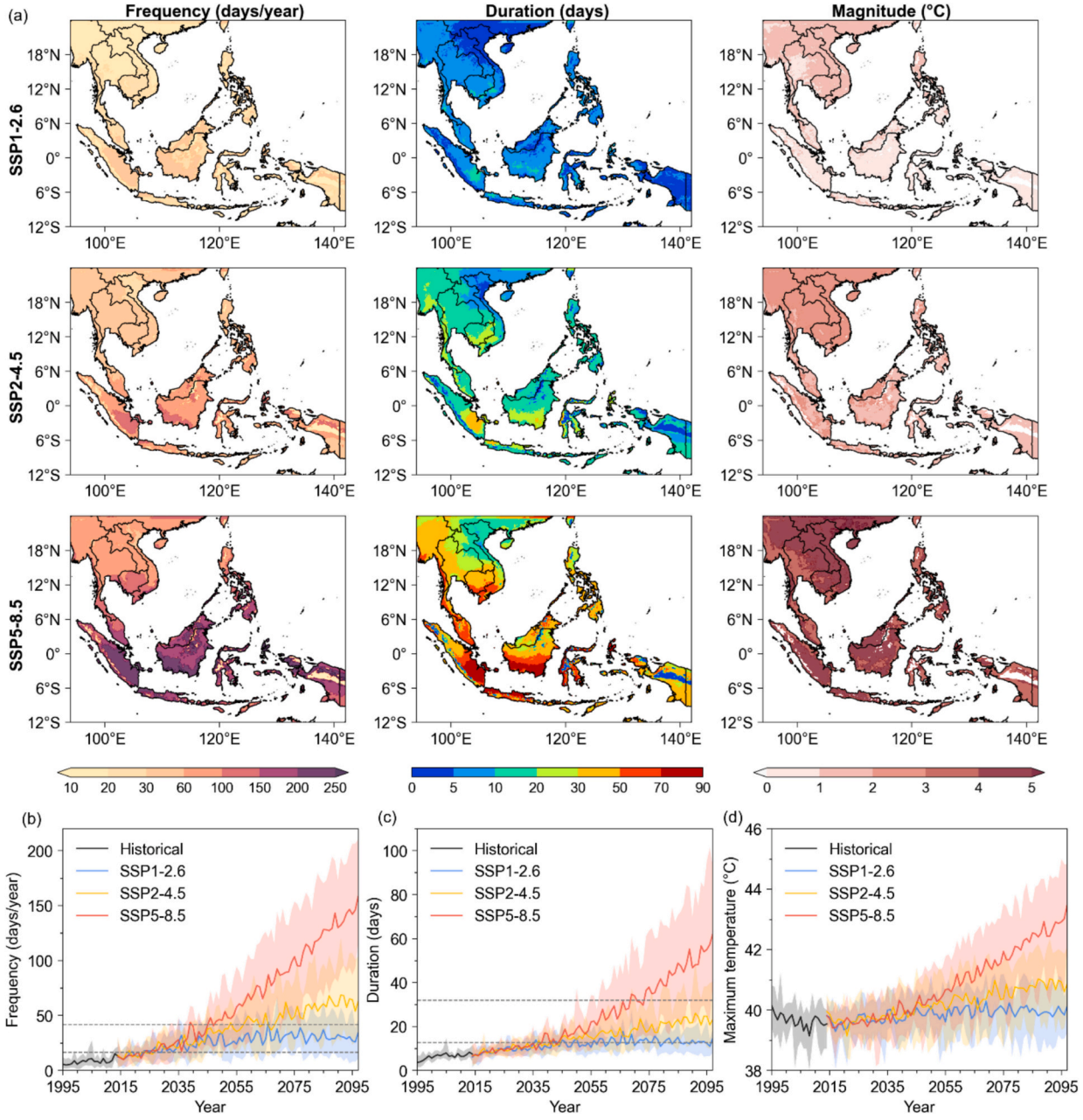

Fig. 5. Projected ensemble mean changes in heatwave frequency (left), duration (middle) and magnitude (right column) for 2080–2099 relative to the baseline period 1995–2014 (a); time series of projected mean (solid line) and ranges (shading) for heatwave frequency (b), duration (c), and magnitude (d) from 1995 to 2099 averaged across Southeast Asia. Dotted lines in (b) and (c) indicate the two and five times of heatwave frequency and duration, respectively, relative to the baseline period 1995–2014.

frequency, duration and magnitude for 2080–2099, scaled in comparison to 2040–2059 (Fig. S3). Under SSP1-2.6, heatwave frequency is expected to increase by 30 days per year in the Indochina and Peninsula Malaysia, and by 60 days per year in most regions of Sumatra and Borneo. The projected increases in heatwave duration range from 5 to 20 days across SEA. Similar to the spatial patterns of projected hotter days, hotspots of higher frequency and longer duration heatwaves are expected in eastern Sumatra, southern Borneo, and northern Java, particularly under the SSP5-8.5 scenario. In these areas, heatwave events are expected to occur for more than 200 days per year and last 70 days longer by the end-century relative to baseline 1995–2014. The Mekong Delta is another concerning hotspot of heatwaves compared to other regions in the Indochina Peninsula, with a projected increase of 120 heatwave days and persistence lasting 50 days longer. The projected increase in heatwave magnitude is comparable to the rise in T_{max} across all SSP scenarios. Spatially, a slightly higher magnitude (i.e., 0.5–1 °C) is projected over the Indochina Peninsula compared to the Maritime Continent under SSP1-2.6 and SSP2-4.5. Under SSP5-8.5, the heatwave magnitude is projected to rise 4 °C across SEA, except in southern Thailand, the Peninsula Malaysia and the Philippines, with a slightly lower increase.

On average across SEA, heatwave frequency, duration and maximum temperature during heatwaves are projected to increase under all the three SSP scenarios until the end of the century (Fig. 5b–d). The differences in these increases are relatively small before 2050s. The projected heatwave frequency and duration are expected to be doubled around 2025 and 2040 relative to the baseline period (1995–2014) across all scenarios, respectively (as shown in dotted lines in Fig. 5b and

c). Under SSP5-8.5, these characteristics escalate significantly in the second half of the century, with heatwave frequency and duration increasing more than fivefold around 2045 and 2070. However, the projected heatwave characteristics stabilize at around 2050 under SSP1-2.6 and around 2080 under SSP2-4.5. This suggests that although carbon mitigation efforts may not take immediate effect in the near future, they will have a substantial impact by the end-century if actions are not taken now.

The evolution of projected heatwave AED, shown in Fig. 6, measures potential future heatwave exposure in SEA countries, taking into account both temporal and spatial scales. By 2050s, the heatwave AED is projected to increase to a level of 20–50 for all the countries and across the three SSP scenarios. However, the trajectories diverge towards the end of the century. Under SSP1-2.6, the AED stabilize after mid-century, while under SSP2-4.5, it continues a mild upward trend until the end of the century to stabilize. In contrast, significant increase in AED is projected in the second half of the century under SSP5-8.5, particularly for Maritime Continent countries (e.g., Brunei, Indonesia, Malaysia and Singapore), where AED could reach in 200. Additionally, the AED curves exhibit more fluctuating and wider range, indicating a higher inter-annual variability and model uncertainty. Notably, in geographically small countries like Brunei and Singapore, which are represented by fewer grid cells in climate models, it is more likely that at least one model will project local temperatures surpassing the heatwave threshold, leading to an earlier occurrence of peak AED (i.e., nearing 365). In contrast, spatial averaging across multiple grid cells in larger countries moderates AED projections. This indicates that the same level of global warming can have disproportional impacts on smaller nations. Given the geographical constraints that limit adaptation opportunities in these countries, early implementation of climate adaptation measure is essential to mitigate heat risks.

3.4. Heat exposure

Fig. 7a presents the ensemble mean CHI and CHT for 16 selected cities (annotated in different colors) across SEA during 2080–2099. Their locations are shown in Fig. 7b, where dot sizes represent projected population density in the 2090s under SSP5, based on Jones and O'Neill (2016). The spatial variation in projected CHI and CHT over SEA under different SSP scenarios and future periods can be found in Fig. S4. These cities are highlighted because they are rapidly growing metropolises with high population density, intensive urban infrastructures, and playing key roles as reginal economic or political centers. Under SSP1-2.6, Hanoi (Vietnam) experiences a higher CHI exceeding 80 °C per year, compared to other cities where CHI ranges between 50 °C and 65 °C. However, CHT remains relatively low at around 140 h per year. This is primarily due to the greater projected temperature increase in northern Vietnam, as shown in Fig. 2c, which plays a crucial role in elevating CHI.

CHI and CHT increase with rising CO_2 levels under SSP2-4.5 and SSP5-8.5. Notably, the CHT rises significantly in cities along the Strait of Malacca (e.g., George Town, Kuala Lumpur, Malacca and Singapore) and on Java (e.g., Jakarta, Bandung and Surabaya). This is driven by an increasing number of hotter days with prolonged time experiencing high temperatures exceeding the threshold. It not only extends the duration of heat exposure, but also amplifies cumulative heat intensity. Particularly, under SSP5-8.5, these cities endure prolonged and intensive extreme heat, with CHT reaching 1000–3000 h/year and CHI levels around 500–600 °C. The values range from 150 to 600 h and 70–130 °C, respectively, during 2040–2059 (Fig. S5). As shown in Fig. 7c, both CHI and CHT increase by 30–70 times compared to the past in these cities, whereas the increase is lower (10–30 times) in Indochina Peninsula cities (e.g., Yangon, Bangkok, and Ho Chi Minh City) and the Philippines

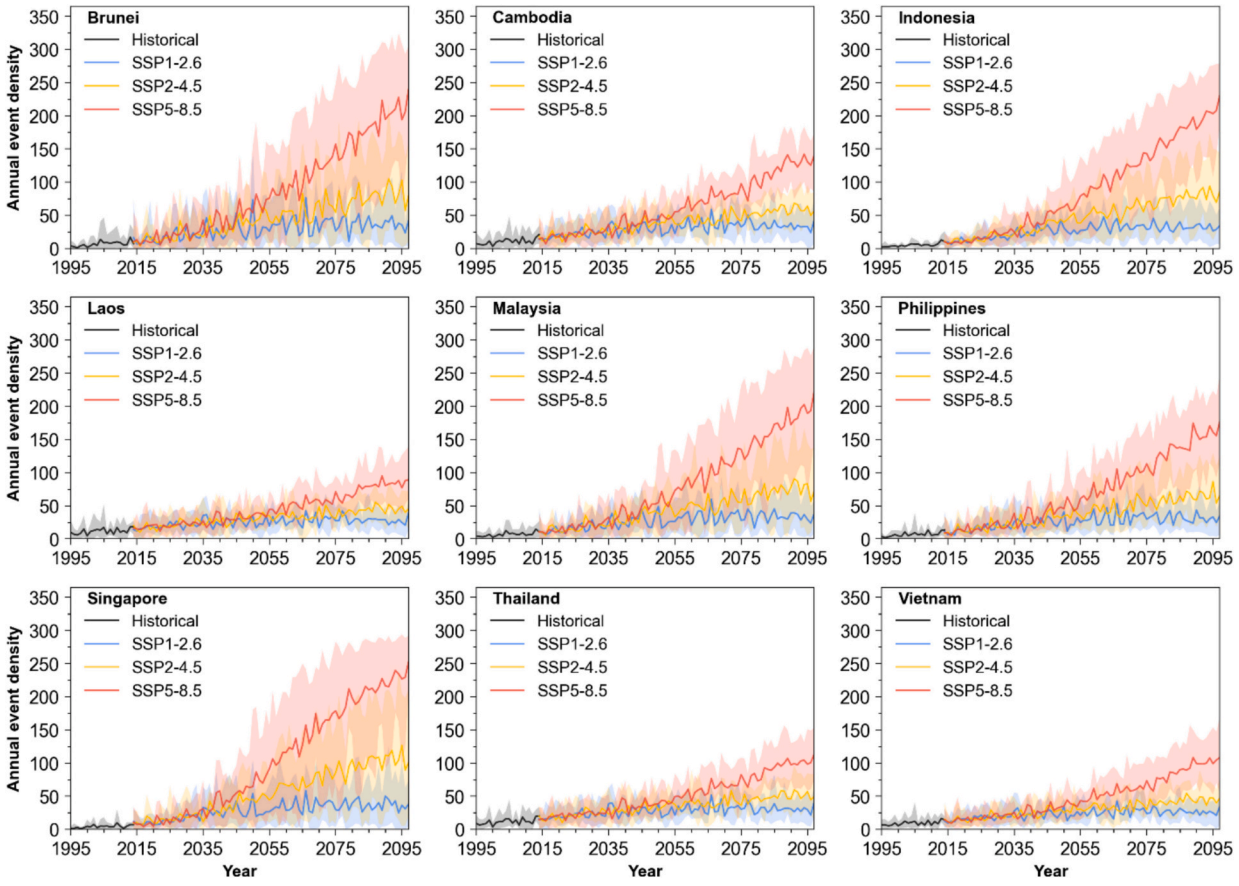

Fig. 6. The projected mean and ranges of time series for annual event density of heatwaves across the nine Southeast Asian countries.

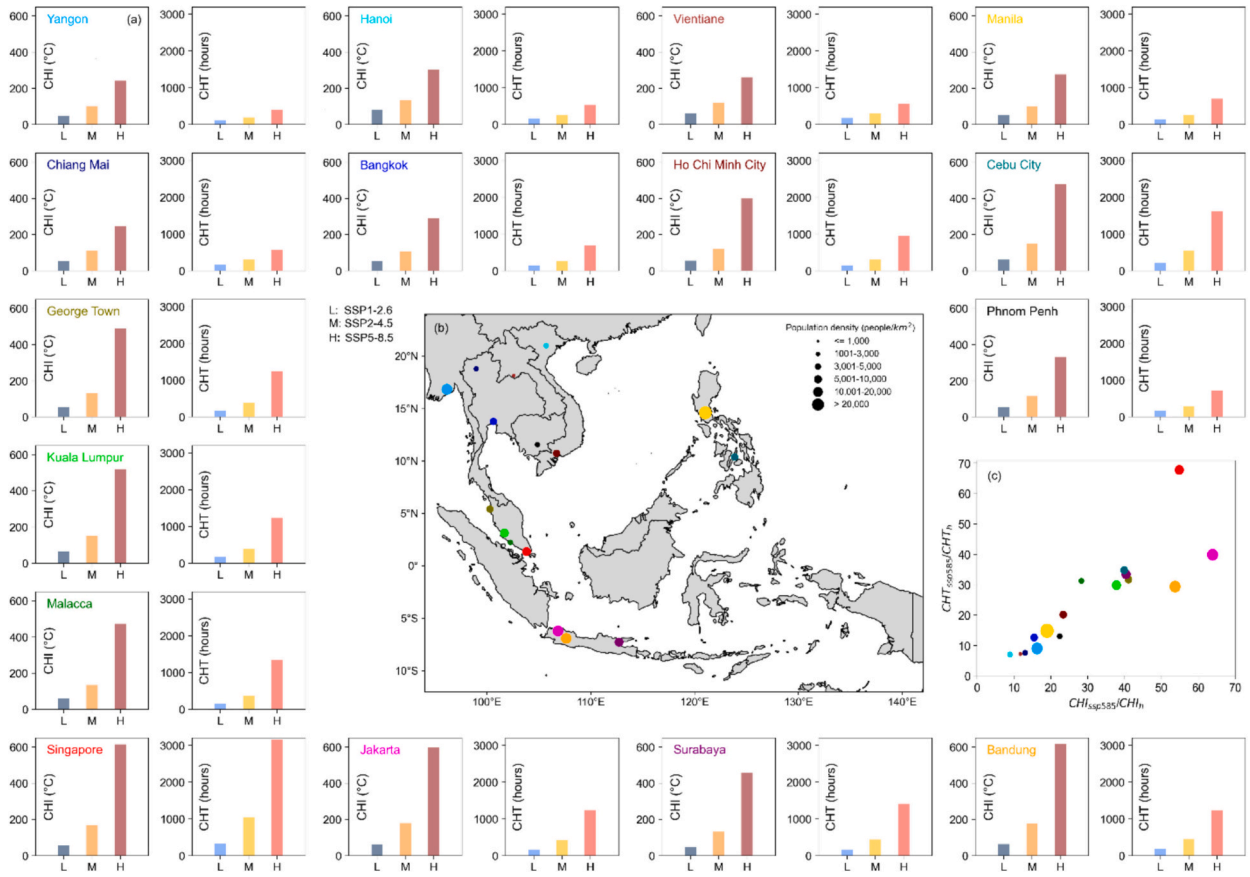

Fig. 7. Projected ensemble mean cumulative heat intensity (CHI, °C) and cumulative heat exposure time (CHT, hours) for 16 Southeast Asian cities during 2080–2099 under SSP1-2.6, SSP2-4.5, and SSP5-8.5 scenarios (a); map of the study cities (b) change ratio of CHI and CHT under SSP5-8.5 relative to the 1995–2014 baseline (c).

(e.g., Manila and Cebu City). However, under SSP1-2.6, the change ratio is only 2–7 times across all selected cities (Fig. S6). This indicates that heat exposure in cities along the Strait of Malacca and on Java is highly sensitive to carbon mitigation efforts. Given the projected high population density over 5000 people/km^2 in these cities, achieving a low-carbon mitigation target, such as SSP1-2.6, could significantly reduce their vulnerability to future extreme heat in terms of both intensity and duration.

4. Discussions

In this study, we primarily investigated ensemble mean changes in future extreme temperatures, heatwaves and heat exposure over SEA using outputs from the high-resolution regional climate model SINGV-RCM, which dynamically downscaled six sub-selected CMIP6 GCMs at 8 km resolution. To the best of our knowledge, this work is the first to report CMIP6 downscaled regional climate projections of heat extremes in this region.

Our findings show an increase of 0.8–1.1 °C, 1.1–1.4 °C, and 1.5–1.9 °C in daily maximum temperatures across nine SEA countries during 2040–2059 under SSP1-2.6, SSP2-4.5 and SSP5-8.5, respectively. The increase further rises to 0.9–1.3 °C, 1.9–2.3 °C, and 3.7–4.5 °C during 2080–2099. In general, a higher increase in daily maximum temperature is projected for countries in the Indochina Peninsula (e.g., Cambodia, Laos, Thailand, and Vietnam), while countries such as Brunei, Indonesia, Malaysia, Philippines, and Singapore are expected to experience more frequent hotter days with daily maximum temperature exceeding the historical 95th percentile threshold. The frequency of projected hotter days in the Maritime Continent accounts for 16–35 % of days in a year during 2040–2059 across the 3 scenarios. It increases significantly by 2080–2099, reaching to 32–47 % and 62–81 % of days in a year under SSP2-4.5 and SSP5-8.5, respectively. This shift represents a new heat norm in SEA's tropical countries by the end of the century, with approximately 4 and 9 months each year, respectively, experiencing temperatures equivalent to or exceeding historical extreme heat events.

The Maritime Continent is characterized by a tropical maritime climate with consistently warm temperature and high humidity. Due to strong oceanic influence, both seasonal and diurnal temperature variability are smaller than those in the Indochina Peninsula, exhibiting a narrower and sharply peaked temperature distribution. Driven by background warming, a slight rightward shift in the future temperature distribution will result in more days being classified as extreme easily when compared to the percentile-based threshold relative to the historical baseline. Moreover, extreme heat events that were historically rare or unprecedented are likely to become more frequent in the future in this region. This change will have disproportional impacts on smaller nations, such as Brunei and Singapore, due to their limited adaptation opportunities, constrained by their geographical size. This also explains why projected heatwave frequency (i.e., annual heatwave days) and duration (i.e., longest heatwave period) are consistently higher and longer in the Maritime Continent compared to the Indochina Peninsula. These findings align with Dong et al. (2021), who analyzed future heatwaves using a large ensemble of CMIP5 GCMs in SEA, despite using a different analysis approach. However, the projected increase in heatwave magnitude (i.e., the increase in maximum temperature during heatwave days) remains relatively uniform across the region.

The high-resolution regional climate projections allow for a detailed examination of heat extremes at regional or city levels. Spatially, the Mekong Delta, eastern Sumatra and southwestern Borneo are identified as hotspots of future temperature increases. In the Mekong Delta, the key

region for rice production in SEA and the world, the extreme heat, along with associated water stress, is expected to frequently threaten crop productivity. Ensuring long-term food resilience will require targeted adaptation measures, including improved cultivation practices, genetic enhancements and advanced irrigation systems. Moreover, as tropical species are already living near the upper limits of their thermal niches (Corlett, 2011), the projected temperature rise in Sumatra and Borneo could potentially push the remaining rainforest ecosystems towards a tipping point, leading to catastrophic consequences such as accelerated forest degradation, severe biodiversity loss and irreversible ecosystem disruptions.

Our study also identifies cities along the Strait of Malacca (e.g., George Town, Kuala Lumpur, Malacca and Singapore) and those on Java (e.g., Jakarta, Bandung and Surabaya) as hotspots exposed to extreme heat in terms of both intensity and duration. These cities already have high population densities and are projected to continue growing. Prolonged heat exposure is expected to pose significant health risks on residents, leading to numerous adverse effects if the heat accumulated in the human body is not sufficiently relieved (Ebi et al., 2021). Moreover, high humidity in the SEA tropics limits the body's ability to dissipate heat, further exacerbating the burden of heat stress in this region. Targeted climate adaptation strategies are necessary, such as ensuring adequate medical resources for the aging population and advising younger generations on behavioral adjustments to cope with escalating heat. It is important to note that the large economic and social disparities across SEA will influence the effectiveness in implementing heat adaptation measures and exacerbate thermal inequality. In this context, regions with high population densities and low incomes in the Maritime Continent (e.g., Indonesia) should be prioritized for support. Overall, achieving carbon mitigation at lower levels can provide substantial benefits for the Maritime Continent, not only for human health but also for agriculture and ecosystems. Nevertheless, to develop tailored climate adaptation policies, it is still crucial to emphasize the need for future studies to quantify the socio-economic and ecological impacts of extreme heat in these identified hotspot regions. Furthermore, developing ultra-high-resolution (e.g., at 100 m resolution) urban climate models is meaningful for assessing city-scale impacts, such as urban heat island effect, and supporting the exploration of additional adaptation opportunities, especially for city-states like Singapore and other megacities in SEA.

This study primarily focuses on interpreting the ensemble mean changes in extreme temperatures, heatwaves and heat exposure. The ensemble mean is a widely used approach in IPCC assessments. By averaging across six RCM simulations, this approach can reduce the biases for single models to provide a more balanced estimation for future projections. However, a key limitation of this approach is that it overlooks individual model performance across different spatial regions. High-resolution gridded temperature observations in SEA that are comparable to our RCM simulations at 8 km resolution remain scarce. This limited availability of observation dataset constraints a comprehensive evaluation of RCM accuracy. To enhance projection reliability, future studies should implement a weighted averaging approach, assigning higher weights to RCM simulations that are superior in historical performance once local observation data become available. Additionally, bias correction is also essential for tailored regional or local studies, especially when absolute temperature thresholds are critical, such as in agriculture and heat stress studies. An alternative strategy to minimize biases from individual models is to drive RCM simulations using boundary conditions derived from the multi-model mean of GCMs. This approach can account for large-scale GCM representations to reduce associated uncertainties.

Nevertheless, the driving GCMs differ in their representation of physical processes, which could lead to divergent regional climate responses and propagate through the RCM simulations. Understanding the inter-model spread of climate change projections is necessary in a risk-based decision making framework in implementing climate adaption strategies. Figs. S7–S10 illustrate the spatial variation in model spread for projected extreme temperatures, heatwaves and heat exposure across RCM simulations under different SSP scenarios and time periods. Despite differences in heat metrics, the spatial patterns are similar. Relatively, the widest model spread is projected in northern Vietnam, followed by Borneo, Sumatra and Peninsula Malayisa, indicating a greater uncertainty in these regions. The level of uncertainty remains comparable through 2040–2059 but increases towards the end of the century, particular under SSP2-4.5 and SSP5-8.5. The presented ensemble mean changes in future extreme heat metrics offer relatively reliable projections for guiding climate adaptation in the mid-century period. However, when applying these results for long-term planning, stakeholders should carefully consider their risk tolerance, especially keeping in mind the heightened uncertainty over the Maritime Continent and under SSP2-4.5 and SSP5-8.5 scenarios.

Furthermore, the high computational cost of regional dynamical downscaling studies often limits the number of GCMs that can be downscaled. Exploring the use of AI techniques to emulate computationally expensive dynamical downscaling is valuable for future research aiming at extending the realizations of regional high-resolution projections to improve robustness and uncertainty estimates.

5. Conclusions

This study presents the first dynamical downscaling of CMIP6 models in Southeast Asia (SEA) under the three SSP scenarios: SSP1-2.6, SSP2-4.5 and SSP5-8.5. It provides high-resolution regional climate projections at 8 km resolution to assess future changes in extreme temperatures, heatwaves and heat exposure. Our results show a significant rise in daily maximum temperatures over SEA, with average increases of 1.0–2.1 °C by 2040–2059 and 1.1–4.0 °C by 2080–2099 across three scenarios. More frequent, prolonged and intense heatwaves are also projected, with heatwave frequency doubling by 2025 and increasing fivefold by 2040 under SSP5-8.5. Heatwave duration is expected to double by 2045 and increase fivefold by 2070 under SSP5-8.5. The Maritime Continent is projected to experience a much higher frequency of extreme heat events by 2080–2099, with approximately 4 and 9 months per year under SSP2-4.5 and SSP5-8.5 respectively, as hot as or hotter than the historical 5 % hottest days.

This high-resolution dynamical downscaling study provides the most granular future projections for SEA, identifying key temperature rising hotspots in the Mekong Delta, eastern Sumatra and southern Borneo. Specifically, cities along the Strait of Malacca and on Java are projected to have heightened exposure to extreme heat, with increased cumulative intensity and prolonged durations. Mitigating emissions along a low-carbon pathway would significantly reduce the risks to human health, agriculture, and ecosystems in the Maritime Continent, particularly in the second half of the century. This study contributes to the growing body of research on future extreme heat and regional dynamical downscaling in SEA, providing critical insights for impact assessments and supporting the development of targeted climate adaption strategies in this highly vulnerable, densely populated region of the world. Future studies are needed to evaluate the regional climate model simulations against the available local observations and adjust the weights used in averaging model outputs to produce more reliable final projections.

CRediT authorship contribution statement

Jianjun Yu: Writing – original draft, Visualization, Software, Methodology, Investigation, Formal analysis, Data curation, Conceptualization. **Aurel F. Moise:** Writing – review & editing, Visualization, Supervision, Project administration, Investigation, Funding acquisition, Conceptualization. **Sandeep Sahany:** Writing – review & editing, Supervision, Project administration, Investigation, Conceptualization. **Venkatraman Prasanna:** Validation, Software. **Xin Rong Chua:** Writing – review & editing, Validation, Software, Resources. **Chen**

Chen: Validation, Software, Resources. **Muhammad E.E. Hassim:** Validation, Resources. **Gerald Lim:** Visualization, Software, Resources, Data curation. **Fei Luo:** Writing – review & editing, Visualization, Investigation, Data curation. **Anupam Kumar:** Writing – review & editing, Investigation, Conceptualization. **Puyang Liu:** Visualization, Software, Investigation, Data curation. **Pavan Harika Raavi:** Data curation.

Declaration of competing interest

The authors declare that they have no known competing financial interests or personal relationships that could have appeared to influence the work reported in this paper.

Acknowledgments

We would like to thank our colleagues at the following centers and agencies for their support in this work: Meteorological Service Singapore, Ministry of Sustainability and the Environment (Singapore), National Supercomputing Centre Singapore, and Bureau of Meteorology (Australia).

Appendix A. Supplementary data

Supplementary data to this article can be found online at https://doi.org/10.1016/j.scitotenv.2025.179501.

Data availability

Singpore's Third National Climate Change Study (V3) data used in this study can be obtained from the V3 Data Sharing Portal, https://v3-climate-projections-uat.mss-int.sg, which is shared under the terms of the Singapore Open Data License version 1.0, https://data.gov.sg/open-data-license.

References

Aadhar, S., Mishra, V., 2023. The 2022 mega heatwave in South Asia in the observed and projected future climate. Environ. Res. Lett. 18 (10), 104011.
Amnuaylojaroen, T., Parasin, N., Limsakul, A., 2024. Projections and patterns of heat-related mortality impacts from climate change in Southeast Asia. Environ. Res. Commun. 6 (3), 035019.
Barriopedro, D., Fischer, E.M., Luterbacher, J., Trigo, R.M., García-Herrera, R., 2011. The hot summer of 2010: redrawing the temperature record map of Europe. Science 332 (6026), 220–224. https://doi.org/10.1126/science.1201224.
Bastos, A., Fu, Z., Ciais, P., Friedlingstein, P., Sitch, S., Pongratz, J., et al., 2020. Impacts of extreme summers on European ecosystems: a comparative analysis of 2003, 2010 and 2018. Philos. Trans. R. Soc. B 375 (1810), 20190507.
Bi, D., Dix, M., Marsland, S., O'Farrell, S., Rashid, H., Uotila, P., et al., 2013. The ACCESS coupled model: description, control climate and evaluation. Austral. Meteorol. Oceanogr. J. 63 (1), 41–64. https://doi.org/10.22499/2.6301.004.
Bush, M., Allen, T., Bain, C., Boutle, I., Edwards, J., Finnenkoetter, A., et al., 2020. The first Met Office Unified Model–JULES regional atmosphere and land configuration, RAL1. Geosci. Model Dev. 13 (4), 1999–2029.
Centre for Climate Research Singapore, National Environment Agency, Singapore, 2024. Singapore's third national climate change study science report. Retrieved from. https://www.mss-int.sg/docs/default-source/v3_reports/v3_science_report/v3-science-report-full.pdf.
Chapman, S., Syktus, J., Trancoso, R., Thatcher, M., Toombs, N., Wong, K.K.H., Takbash, A., 2023. Evaluation of dynamically downscaled CMIP6-CCAM models over Australia. Earth Fut. 11 (11) e2023EF003548.
Coates, L., van Leeuwen, J., Browning, S., Gissing, A., Bratchell, J., Avci, A., 2022. Heatwave fatalities in Australia, 2001–2018: an analysis of coronial records. Int. J. Dis. Risk Reduct. 67, 102671.
Corlett, R.T., 2011. Impacts of warming on tropical lowland rainforests. Trends Ecol. Evol. 26 (11), 606–613.
Domeisen, D.I., Eltahir, E.A., Fischer, E.M., Knutti, R., Perkins-Kirkpatrick, S.E., Schär, C., et al., 2023. Prediction and projection of heatwaves. Nat. Rev. Earth Environ. 4 (1), 36–50. https://doi.org/10.1038/s43017-022-00371-z.
Dong, Z., Wang, L., Sun, Y., Hu, T., Limsakul, A., Singhruck, P., Pimonsree, S., 2021. Heatwaves in Southeast Asia and their changes in a warmer world. Earth Fut. 9 (7). https://doi.org/10.1029/2021EF001992 e2021EF001992.
Döscher, R., Acosta, M., Alessandri, A., Anthoni, P., Arsouze, T., Bergman, T., et al., 2022. The EC-Earth3 earth system model for the coupled model intercomparison project 6. Geosci. Model Dev. 15, 2973–3020.
Ebi, K.L., Capon, A., Berry, P., Broderick, C., de Dear, R., Havenith, G., et al., 2021. Hot weather and heat extremes: health risks. Lancet 398 (10301), 698–708.
Forzieri, G., Bianchi, A., Batista e Silva, F., Herrera, M.A.M., Leblois, A., Lavalle, C., et al., 2018. Escalating impacts of climate extremes on critical infrastructures in Europe. Glob. Environ. Chang. 48, 97–107.
Gibson, P.B., Stuart, S., Sood, A., Stone, D., Rampal, N., Lewis, H., et al., 2024. Dynamical downscaling CMIP6 models over New Zealand: added value of climatology and extremes. Clim. Dyn. 62 (8), 8255–8281.
Giorgi, F., Jones, C., Asrar, G.R., 2009. Addressing climate information needs at the regional level: the CORDEX framework. World Meteorol. Org. Bull. 58 (3), 175.
Gutjahr, O., Putrasahan, D., Lohmann, K., Jungclaus, J.H., von Storch, J.S., Brüggemann, N., et al., 2019. Max planck institute earth system model (MPI-ESM1.2) for the high-resolution model intercomparison project (HighResMIP). Geosci. Model Dev. 12 (7), 3241–3281. https://doi.org/10.5194/gmd-12-3241-2019.
Gutowski Jr., W.J., Giorgi, F., Timbal, B., Frigon, A., Jacob, D., Kang, H.S., et al., 2016. WCRP coordinated regional downscaling experiment (CORDEX): a diagnostic MIP for CMIP6. Geosci. Model Dev. 9, 4087–4095. https://doi.org/10.5194/gmd-9-4087-2016.
Hagemann, S., Chen, C., Clark, D.B., Folwell, S., Gosling, S.N., Haddeland, I., et al., 2013. Climate change impact on available water resources obtained using multiple global climate and hydrology models. Earth Syst. Dynam. 4 (1), 129–144. https://doi.org/10.5194/esd-4-129-2013.
Hansen, J., Sato, M., Ruedy, R., Lo, K., Lea, D.W., Medina-Elizade, M., 2006. Global temperature change. Proc. Natl. Acad. Sci. 103 (39), 14288–14293. https://doi.org/10.1073/pnas.0606291103.
IPCC, 2021. Summary for policymakers. In: Climate Change 2021: The Physical Science Basis. Contribution of Working Group I to the Sixth Assessment Report of the Intergovernmental Panel on Climate Change. Cambridge University Press, Cambridge, United Kingdom and New York, NY, USA, pp. 3–32. https://doi.org/10.1017/9781009157896.001.
Jones, B., O'Neill, B.C., 2016. Spatially explicit global population scenarios consistent with the Shared Socioeconomic Pathways. Environ. Res. Lett. 11 (8), 084003. https://doi.org/10.1088/1748-9326/11/8/084003.
Ke, X., Wu, D., Rice, J., Kintner-Meyer, M., Lu, N., 2016. Quantifying impacts of heat waves on power grid operation. Appl. Energy 183, 504–512.
Kim, J.H., Nam, S.H., Kim, M.K., Serrano-Notivoli, R., Tejedor, E., 2024. The 2022 record-high heat waves over southwestern Europe and their underlying mechanism. Weather Clim. Extr. 46, 100729.
Lesk, C., Anderson, W., Rigden, A., Coast, O., Jägermeyr, J., McDermid, S., et al., 2022. Compound heat and moisture extreme impacts on global crop yields under climate change. Nat. Rev. Earth Environ. 3 (12), 872–889. https://doi.org/10.1038/s43017-022-00368-8.
Li, X.X., 2020. Heat wave trends in Southeast Asia during 1979–2018: The impact of humidity. Sci. Total Environ. 721, 137664.
Liu, J., Ren, Y., Tao, H., Shalamzari, M.J., 2021. Spatial and temporal variation characteristics of heatwaves in recent decades over China. Remote Sens. 13 (19), 3824.
Liu, L., Qin, X., 2023. Analysis of heatwaves based on the universal thermal climate index and apparent temperature over mainland Southeast Asia. Int. J. Biometeorol. 67 (12), 2055–2068.
Lyu, Y., Wang, J., Zhi, X., Wang, X., Zhang, H., et al., 2024. The characterization, mechanism, predictability, and impacts of the unprecedented 2023 Southeast Asia heatwave. npj Clim. Atmos. Sci. 7 (1), 246.
Mora, C., Dousset, B., Caldwell, I.R., Powell, F.E., Geronimo, R.C., Bielecki, C.R., et al., 2017. Global risk of deadly heat. Nat. Clim. Chang. 7 (7), 501–506. https://doi.org/10.1038/nclimate3322.
Muhammad, M.K.I., Hamed, M.M., Harun, S., Sa'adi, Z., Sammen, S.S., Al-Ansari, N., et al., 2024. Heatwaves in Peninsular Malaysia: a spatiotemporal analysis. Sci. Rep. 14 (1), 4255.
Nguyen, P.L., Alexander, L.V., Thatcher, M.J., Truong, S.C., Isphording, R.N., McGregor, J.L., 2024. Selecting CMIP6 global climate models (GCMs) for Coordinated Regional Climate Downscaling Experiment (CORDEX) dynamical downscaling over Southeast Asia using a standardised benchmarking framework. Geosci. Model Dev. 17 (19), 7285–7315. https://doi.org/10.5194/gmd-17-7285-2024.
Nik, V.M., Perera, A.T.D., Chen, D., 2021. Towards climate resilient urban energy systems: a review. Natl. Sci. Rev. 8 (3), nwaa134. https://doi.org/10.1093/nsr/nwaa134.
Perera, A.T.D., Nik, V.M., Chen, D., Scartezzini, J.L., Hong, T., 2020. Quantifying the impacts of climate change and extreme climate events on energy systems. Nat. Energy 5 (2), 150–159. https://doi.org/10.1038/s41560-020-0558-0.
Perkins, S.E., 2015. A review on the scientific understanding of heatwaves—their measurement, driving mechanisms, and changes at the global scale. Atmos. Res. 164, 242–267.
Perkins-Kirkpatrick, S.E., Lewis, S.C., 2020. Increasing trends in regional heatwaves. Nat. Commun. 11 (1), 3357.
Prasanna, V., Dipankar, A., Liu, J., Lim, G., Moise, A., Chua, X.R., et al., 2024. SINGV-RCM: the convection-permitting regional climate model for Singapore. Clim. Dyn. 1–13.
Racherla, P.N., Shindell, D.T., Faluvegi, G.S., 2012. The added value to global model projections of climate change by dynamical downscaling: a case study over the continental US using the GISS-ModelE2 and WRF models. J. Geophys. Res. Atmos. 117 (D20). https://doi.org/10.1029/2012JD018091.

Ridder, N.N., Ukkola, A.M., Pitman, A.J., Perkins-Kirkpatrick, S.E., 2022. Increased occurrence of high impact compound events under climate change. Npj Clim. Atmos. Sci. 5 (1), 3. https://doi.org/10.1038/s41612-021-00224-4.

Robine, J.M., Cheung, S.L.K., Le Roy, S., Van Oyen, H., Griffiths, C., Michel, J.P., Herrmann, F.R., 2008. Death toll exceeded 70,000 in Europe during the summer of 2003. C. R. Biol. 331 (2), 171–178. https://doi.org/10.1016/j.crvi.2007.12.001.

Ruthrof, K.X., Breshears, D.D., Fontaine, J.B., Froend, R.H., Matusick, G., Kala, J., et al., 2018. Subcontinental heat wave triggers terrestrial and marine, multi-taxa responses. Sci. Rep. 8 (1), 13094. https://doi.org/10.1038/s41598-018-31236-5.

Seland, Ø., Bentsen, M., Olivié, D., Toniazzo, T., Gjermundsen, A., Graff, L.S., et al., 2020. Overview of the Norwegian Earth System Model (NorESM2) and key climate response of CMIP6 DECK, historical, and scenario simulations. Geosci. Model Dev. 13 (12), 6165–6200. https://doi.org/10.5194/gmd-13-6165-2020.

Senior, C.A., Jones, C.G., Wood, R.A., Sellar, A., Belcher, S., Klein-Tank, A., Mulcahy, J. P., 2020. UK community earth system modeling for CMIP6. J. Adv. Model. Earth Syst. 12 (9) e2019MS002004.

Sun, X., Ge, F., Fan, Y., Zhu, S., Chen, Q., 2022. Will population exposure to heat extremes intensify over Southeast Asia in a warmer world? Environ. Res. Lett. 17 (4), 044006.

Sun, X., Ge, F., Chen, Q., Fraedrich, K., Li, X., 2023. How striking is the intergenerational difference in exposure to compound heatwaves over Southeast Asia? Earth Fut. 11 (6) e2022EF003179.

Tangang, F., Chung, J.X., Juneng, L., Supari, Salimun, E., Ngai, S.T., Kumar, P., 2020. Projected future changes in rainfall in Southeast Asia based on CORDEX–SEA multi-model simulations. Clim. Dyn. 55, 1247–1267.

Tatebe, H., Ogura, T., Nitta, T., Komuro, Y., Ogochi, K., Takemura, T., et al., 2019. Description and basic evaluation of simulated mean state, internal variability, and climate sensitivity in MIROC6. Geosci. Model Dev. 12 (7), 2727–2765.

Thirumalai, K., DiNezio, P.N., Okumura, Y., Deser, C., 2017. Extreme temperatures in Southeast Asia caused by El Niño and worsened by global warming. Nat. Commun. 8 (1), 15531. https://doi.org/10.1038/ncomms15531.

Thompson, V., Kennedy-Asser, A.T., Vosper, E., Lo, Y.E., Huntingford, C., Andrews, O., et al., 2022. The 2021 western North America heat wave among the most extreme events ever recorded globally. Sci. Adv. 8 (18), eabm6860.

Van Den Besselaar, E.J., Van Der Schrier, G., Cornes, R.C., Iqbal, A.S., Klein Tank, A.M., 2017. SA-OBS: a daily gridded surface temperature and precipitation dataset for Southeast Asia. J. Clim. 30 (14), 5151–5165.

Vautard, R., van Aalst, M., Boucher, O., Drouin, A., Haustein, K., Kreienkamp, F., et al., 2020. Human contribution to the record-breaking June and July 2019 heatwaves in Western Europe. Environ. Res. Lett. 15 (9), 094077. https://doi.org/10.1088/1748-9326/aba3d4.

Wilks, D.S., 2011. Statistical Methods in the Atmospheric Sciences. Academic Press.

Yiou, P., Cattiaux, J., Faranda, D., Kadygrov, N., Jézéquel, A., Naveau, P., et al., 2020. Analyses of the Northern European summer heatwave of 2018. Bull. Am. Meteorol. Soc. 101 (1), S35–S40. https://doi.org/10.1175/BAMS-D-19-0170.1.

Yoon, A., Kim, J., Lee, J., Sung, H.M., Hong, J.W., Min, S.K., et al., 2024. Factor analysis of recent major heatwaves in East Asia. Geosci. Front. 15 (1), 101730.

Zhu, T., Fonseca De Lima, C.F., De Smet, I., 2021. The heat is on: how crop growth, development, and yield respond to high temperature. J. Exp. Bot. 72 (21), 7359–7373. https://doi.org/10.1093/jxb/erab308.

Zobel, Z., Wang, J., Wuebbles, D.J., Kotamarthi, V.R., 2017. High-resolution dynamical downscaling ensemble projections of future extreme temperature distributions for the United States. Earth's Future 5 (12), 1234–1251. https://doi.org/10.1002/2017EF000642.